Engineering Analysis with Boundary Elements 37 (2013) 699–707

Contents lists available at SciVerse ScienceDirect

Engineering Analysis with Boundary Elements

journal homepage: www.elsevier.com/locate/enganabound

A coupled BEM-stiffness matrix approach for analysis of shear deformable plates on elastic half space

Ahmed Mostafa Shaaban [a], Youssef F. Rashed [b,*]

[a] Bridges and Special Structures Department, Dar Al-Handasah, Mohandessin, Giza, Egypt
[b] Deputy Secretary General, Supreme Council of Universities, Egypt and Structural Engineering Department, Cairo University, Giza, Egypt

ARTICLE INFO

Article history:
Received 29 March 2012
Accepted 21 December 2012

Keywords:
Boundary element method
Elastic half space
Plates
Stiffness matrix
Reissner plates

ABSTRACT

In this paper, a new direct Boundary Element Method (BEM) is presented to solve plates on elastic half space (EHS). The considered BEM is based on the formulation of Vander Weeën for the shear deformable plate bending theory of Reissner. The considered EHS is the infinite EHS of Boussinesq–Mindlin or the finite EHS (with rigid end layer) of Steinbrenner. The multi-layered EHS is also considered. In the present formulation, the soil stiffness matrix is computed. Hence, this stiffness matrix is directly incorporated inside the developed BEM. Several numerical examples are considered and results are compared against previously published analytical and numerical methods to validate the present formulation.

1. Introduction

In structural designs, soil-structural interaction problem is always point of research where good representation is necessary. One of the most common methods in design companies is the Winkler spring method [1]. It is based on representing the soil as individual springs. Such a model assumes the displacement of soil medium at any surface point to be directly proportional to the applied stress and independent of stresses applied to other locations. The displacement occurs immediately under the loaded area; whereas displacement outside this region is zero. The Winkler method is mainly dependent on accurate determination of the coefficient of sub-grade reaction [2]. There is a large range of sub-grade reaction values produced from many methods such as experienced charts and methods based on the theory of elasticity [2]. The Winkler method does not consider coupling between springs through soil layers but relies on the attached footing stiffness [2]. Moreover, the Winkler method does not take soil layering and most engineers rely on the surface layer properties or properties of an equivalent layer. Although this method dates many decades, it is still used until now because of its simplicity.

The two-parameter elastic models have been developed as refined soil representations. These models use pre-defined two independent elastic constants. Some of these models provide mechanical interaction between Winkler individual springs using elastic membrane, elastic beams, or elastic layers that carry soil shear deformations. Examples of such models are the work of Filonenko-Borodich [3,4], Hetenyi [5], Pasternak [6] and Kerr [7]. Other two-parameter models are based on simplified assumptions to the original elastic continuum model, such as the models of Reissner [8] and Vlasov and Leontiev [9].

It has to be noted that, the sub-grade reaction modulus and other soil parameters are not mechanical soil properties [2] but they depend on the shape and the load pattern of the loaded area.

The ACI committee [10] suggested using an elastic half space technique with the Boussinesq theory instead of the Winkler model for accurate modeling. Unlike the Winkler and the two-parameter models, the elastic half space method uses data obtained from geotechnical investigations.

There are many models that treat soil as an elastic half space. Among them are the models of Boussinesq [11] and Mindlin [12], which consider the soil as an elastic, isotropic, homogenous, and infinite half space. The Steinbrenner elastic half space model [13], on the other hand, considers presence of a rigid layer under the considered surface soil finite layer. Another method that analyzes the soil under plates is the finite layer method [14] in which the soil is divided into several horizontal layers.

Plates resting on elastic half space are studied with the finite element method and the boundary element method besides presence of some analytical solutions. This is considering thin and thick plate theories. The application of the BEM to plate bending problems modeled using the thin plate theory was introduced by Bézine [15] and Stern [16]. Vander Weeën [17] derived a BEM for plate bending problems based on the shear deformable plate theory according to Reissner [18]. In the last 20

* Corresponding author. Tel.: +20 100 511 2949.
E-mail addresses: youssef@eng.cu.edu.eg, yrashed@bue.edu.eg (Y.F. Rashed).

0955-7997/$ - see front matter © 2012 Elsevier Ltd. All rights reserved.
http://dx.doi.org/10.1016/j.enganabound.2012.12.005

years, the formulation of Vander Weeën [17] became a standard formulation among researchers due to its stability and versatility. The edited book of Aliabadi [19] contained several advanced developments in BEM for plate bending problems using Vander Weeën formulation. Rashed [20] extended the formulation of Vander Weeën [17] to solve practical rafts on Winkler foundation.

Several researches have discussed the analysis of plates on elastic half space. Selvadurai [11], Bowels [13], and Das [21] proposed different methods of elastic analysis of soil–plate interaction. Hemsley [22] proposed an elastic solution for axisymmetrically loaded circular plate with free and clamped edges on Winkler springs and on a half-space. Chen and Peng [23] demonstrated a finite element computation of plates on elastic half space for various base-models. Timoshenko and Goddier [24] also discussed few methods for soil–plate analysis based on the theory of elasticity. Wang et al. [25] used bending of plates on an elastic half-space analyzed by isoprametric finite elements. Wardle and Fraser [26] carried out a finite element analysis of a plate on a layered cross-anisotropic elastic half space. They also discussed a numerical analysis of rectangular plates on layered elastic half space in Ref. [27]. Ta and Small [14] carried out an analysis of plates modeled by FEM on finite layered half space with full analysis and another analysis uses some approximations. Stavridis [28] proposed a simplified analysis of layered soil-structure interaction. Wang et al. [12] provided an analysis of rectangular thick plates on an elastic half space using Ritz method. Wang et al. [29] demonstrated a plate on layered elastic half space analyzed by a semi-analytical and semi-numerical method.

Considering the boundary element modeling for plates on elastic half space, Syngellakis and Bai [30] discussed the application of the boundary element method to thin plate on the Boussinesq half space. Xiao [31] analyzed thick plates on elastic half space using special form of the indirect boundary integral formulation where in his analysis; results are obtained in terms of two Hu functions [32] with no reference to physical variables. The formulation of Xiao [31] produces hyper-singular kernels in the integral equations. Therefore, in Ref. [31], the collocation points are placed outside the boundary together with using constant elements to avoid hyper-singular integrals. This leads to limit the application of the method presented in Ref. [31] to small problems of no practical use.

This paper presents a new practical technique of using the Boundary Element Method (BEM) to solve plates on elastic half space. The considered BEM is based on the formulation of Vander Weeën [17] for the shear deformable plate bending theory. The considered EHS is the infinite EHS of Boussinesq–Mindlin or the finite EHS (with rigid end layer) of Steinbrenner. The multi-layered EHS is also considered. In the present formulation, the soil stiffness matrix is computed. Hence, this stiffness matrix is directly incorporated inside the developed BEM.

Several numerical examples are presented and results are compared against previously published analytical and numerical methods to validate the present formulation.

2. Stiffness matrix for multi-layered elastic half space

In this section, the stiffness matrix of the elastic half space is formed and modified to be ready to be fit into the proposed BEM formulation in the next section.

2.1. Elasticity solutions

In this section, elastic solutions of Boussinesq, Mindlin and Steinbrenner are reviewed. The EHS boundary (surface under the plate) is divided into *Nc* area segments at which the displacement is required to be computed in any segment due to loading at the origin. The following sub-sections compute the flexibility matrix of the overall EHS divisions.

2.1.1. Bousinessq solution

The displacement $w_{(X,Y)}$ of a point lying on the surface of an elastic, isotropic, homogenous and infinite thickness half space due to a concentrated load P acting at the origin (0, 0) is [11]

$$w_{(X,Y)} = \frac{(1-\nu)P}{2\pi G r} \tag{1}$$

in which $G = E/2(1+\nu)$ is the shear modulus, E is the modulus of elasticity, ν is the Poisson's ratio and

$$r = \sqrt{X^2+Y^2}.$$

In order to avoid singularity under loading when computing $w_{(0,0)}$, the concentrated loading is replaced by equivalent pressure of intensity q over circular area of radius a [11], to give

$$w_{(0,0)} = \frac{(1-\nu)qa}{G} \tag{2}$$

2.1.2. Mindlin solution

Similar to Bousinessq solution, Mindlin solution considers similar equation to Eq. (1) for the surface displacement $w_{(X,Y)}$ at distance $r = \sqrt{X^2+Y^2}$. However, displacement under load is computed by integrating the equivalent uniform load over rectangular area $(B \times L)$ to give [12]

$$w_{(0,0)} = \frac{P}{8\pi G(1-\nu)B}\left((3-4\nu)\left(\beta \ln\left(\frac{1+\sqrt{1+\beta^2}}{\beta}\right)+\ln\left(\beta+\sqrt{1+\beta^2}\right)\right) + (5-12\nu-8\nu^2)\left(\beta \ln\left(\frac{1+\sqrt{1+\beta^2}}{\beta}\right)+\ln\left(\beta+\sqrt{1+\beta^2}\right)\right)\right) \tag{3}$$

in which $\beta = B/L$.

It has to be noted that, displacement values computed from both Boussinesq and Mindlin solutions could be multiplied by a factor to account for the presence of rigid layer at limited depths [21].

2.1.3. Steinbrenner solution

It considers the displacement w of a rectangular loaded area of dimension $B \times L$ on the surface of elastic half space having a finite soil layer underneath the plate. Such a soil layer is above a rigid layer. The displacement is computed based on theory of elasticity as follow [13]:

$$w = qB\frac{1-\nu^2}{E} m\left(I_1 + \frac{1-2\nu}{1-\nu} I_2\right) I_F \tag{4}$$

where q is the equivalent uniform applied stress over the loaded area $(B \times L)$, E is the modulus of elasticity and ν is the Poisson's ratio. I_1 and I_2 are influence factors computed using equations given by Steinbrenner [13] as follow:

$$I_1 = \frac{1}{\pi}\left(M \ln \frac{\left(1+\sqrt{M^2+1}\right)\sqrt{M^2+N^2}}{M\left(1+\sqrt{M^2+N^2+1}\right)} + \ln \frac{\left(M+\sqrt{M^2+1}\right)\sqrt{1+N^2}}{M+\sqrt{M^2+N^2+1}}\right) \tag{5}$$

$$I_2 = \frac{N}{2\pi} \tan^{-1}\left(\frac{M}{N\sqrt{M^2+N^2+1}}\right) \tag{6}$$

in which $M = L/B$, $N = H/B$ and H is the height of the soil layer above the rigid layer. I_F is the influence factor depending on plate embedment depth D, in this work, I_F is taken to be $=1$ as all considered plates in this paper are located on the EHS surface. m is the number of corners contributing to displacement w. At the

plate center $m=4$, at a side point $m=2$ and at a corner point $m=1$.

2.2. Displacement calculation due to multi-layered elastic half space (Stavridis [28])

In this work, the method of Stavridis [28] to compute displacement of multi-layered elastic half space is used. The EHS is considered to be consisted of a finite number k of horizontal layers over a rigid layer. Each layer i is defined by the distance

Z_i measured from the EHS surface to the lower surface of the layer and its elastic parameters are (E_i,υ_i). The displacement of a point S w_s on a multi-layered EHS may be considered as the superposed contribution of its layers $w_{s,i}(E_i,\upsilon_i)$ as follows [28]:

$$w_s = w_{s,1}(E_1,\upsilon_1)+w_{s,2}(E_2,\upsilon_2)+w_{s,3}(E_3,\upsilon_3)+\ \ldots\ldots\ldots\ldots+w_{s,k}(E_k,\upsilon_k) \tag{7}$$

where

$$w_{s,i}(E_i,\upsilon_i) = w_s(Z_i,E_i,\upsilon_i)-w_s(Z_{i-1},E_i,\upsilon_i) \tag{8}$$

after substituting Eq. (8) into Eq. (7) the surface displacement could be obtained as follows:

$$\begin{aligned} w_s = {} & w_s(Z_1,E_1,\upsilon_1)+(w_s(Z_2,E_2,\upsilon_2)- w_s(Z_1,E_2,\upsilon_2)) \\ & + (w_s(Z_3,E_3,\upsilon_3)-w_s(Z_2,E_3,\upsilon_3))+\ \ldots\ldots\ldots\ldots \\ & + (w_s(Z_k,E_k,\upsilon_k)-w_s(Z_{k-1},E_k,\upsilon_k)) \end{aligned} \tag{9}$$

2.3. Computation of soil flexibility and stiffness matrices

The EHS part under the plate is divided into Nc area segments in both of the X and the Y directions as shown in Fig. 1. Each segment is loaded in its center by a vertical concentrated unit load. This unit load is uniformly distributed over the segment area. The resulting displacements at all segment centers are computed using any of the previously mentioned displacement Eqs. (1)–(4) or (9) for multi-layered EHS. All obtained displacement values are arranged in a matrix form such that each load case is arranged in a single column to form the soil flexibility matrix $[F]_{Nc\times Nc}$.

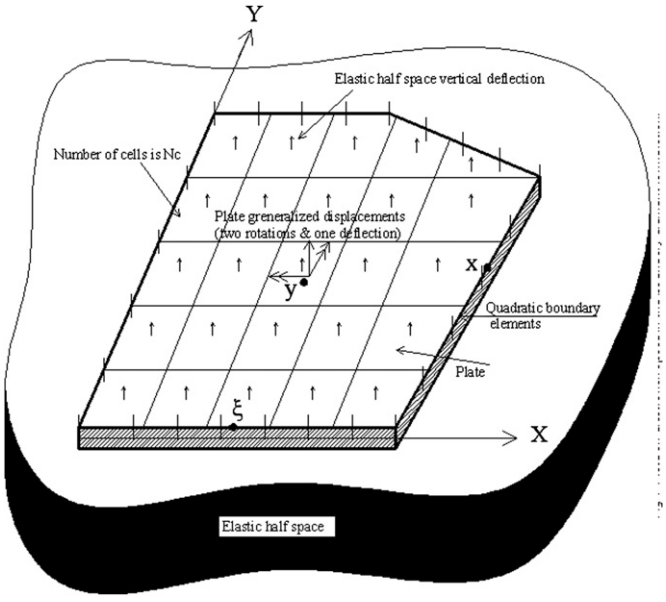

Fig. 1. Plate on elastic half space in the boundary element formulation.

The soil stiffness matrix $[K]_{Nc\times Nc}$ can be considered as the inverse of the soil flexibility matrix, i.e.

$$[K]_{Nc\times Nc} = [F]^{-1}{}_{Nc\times Nc} \tag{10}$$

3. The proposed BEM for plate on elastic half space

Consider an arbitrary plate of domain Ω and boundary Γ. The plate is lying in the x_1-x_2 (X–Y) plane where $x_3=0$ is located at the mid surface of the plate as shown in Fig. 1. The indecial notation is used in this section where the Greek indexes vary from 1 to 2 and Roman indexes vary from 1 to 3. The Reissner plate bending theory [18] is used in the present formulation, which is suitable to model engineering foundations. The direct boundary integral equation for such a plate can be written in the following form (in the absence of body forces and domain loadings) [17]:

$$C_{ij}(\xi)u_j(\xi)+\int_{\Gamma(x)} T_{ij}(\xi,x)u_j(x)d\Gamma(x) = \int_{\Gamma(x)} U_{ij}(\xi,x)t_j(x)d\Gamma(x) \tag{11}$$

where $T_{ij}(\xi,x)$, $U_{ij}(\xi,x)$ are the two-point fundamental solution kernels for tractions and displacements respectively [17]. The two points ξ and x are the source and the field points respectively. $u_j(x)$ and $t_j(x)$ denote the boundary generalized displacements (two rotations u_α and vertical deflection $u_3=w$) and tractions. $C_{ij}(\xi)$ is the jump term. The symbols ν and λ denote the plate Poison's ratio and shear factor.

If the plate domain is placed over elastic half space, and both the plate domain and the elastic half space domain (under the plate domain) are discretized into c internal cells ($c=Nc$), at which the half space reaction is considered to vary constantly, the boundary integral equation in (11) could be re-written as follows:

$$\begin{aligned} C_{ij}(\xi)u_j(\xi)+\int_{\Gamma(x)} T_{ij}(\xi,x)u_j(x)d\Gamma(x) = {} & \int_{\Gamma(x)} U_{ij}(\xi,x)t_j(x)d\Gamma(x) \\ & +\sum_c \left\{ \int_{\Omega_c(y)} \left[U_{i3}(\xi,y)-\frac{\nu}{(1-\nu)\lambda^2}U_{i\alpha,\alpha}(\xi,y)\right] d\Omega_c(y)P_3(y)\right\} \end{aligned} \tag{12}$$

where the P_3 denotes the unknown interaction forces between the soil cells and the plate internal cells. The new field point y denotes the point of the soil internal cell center. In such a case, another set of integral equations could be written at each soil internal cell centers y to give

$$\begin{aligned} u_i(Y)+\int_{\Gamma(x)} T_{ij}(Y,x)u_j(x)d\Gamma(x) = {} & \int_{\Gamma(x)} U_{ij}(Y,x)t_j(x)d\Gamma(x) \\ & +\sum_c \left\{ \int_{\Omega_c(y)} \left[U_{ik}(Y,y)-\frac{\nu}{(1-\nu)\lambda^2}U_{i\alpha,\alpha}(Y,y)\right] d\Omega_c(y)P_3(y)\right\} \end{aligned} \tag{13}$$

where Y is a new source point located at each soil cell center and could denote any of the y points.

After discretizing the plate boundary to NE quadratic boundary elements with N boundary nodes and the plate internal soil cells to Nc, Eqs. (12) and (13) could be re-written in matrix form as follows:

$$\begin{bmatrix} [A]_{3N\times 3N} & [0] & [A_2]_{3N\times 3N_c} \\ [A_1]_{3N_c\times 3N} & [I] & [A_3]_{3N_c\times 3N_c} \end{bmatrix} \begin{Bmatrix} \{u/t\}_{3N\times 1} \\ \{u_c\}_{3N_c\times 1} \\ \{P\}_{3N_c\times 1} \end{Bmatrix} = \begin{Bmatrix} \{RHS_b\}_{3N\times 1} \\ \{RHS_c\}_{3N_c\times 1} \end{Bmatrix} \tag{14}$$

where the matrix $[A]$ and the vector $\{RHS_b\}$ denote the well-known matrix of coefficients and the right hand side vector of prescribed values due to collocation at a boundary point and after applying the boundary conditions (recall Eqs. (11) or (12)) [17]. The Matrix $[A_1]$ together with the vector $\{RHS_c\}$ are similar identities to the matrix $[A]$ and the vector $\{RHS_b\}$ but when

collocating at internal soil cell center (recall Eq. (13)). The matrix $[A_2]$ contains negative values of coefficients computed from the second integral on the right hand side of Eq. (12). Similar to $[A_2]$, the matrix $[A_3]$ contains negative values of coefficients computed from the second integral on the right hand side of Eq. (13) after adding the identity matrix to it (due to the free term $u_i(Y)$ on the left hand side of Eq. (13)). The vector $\{u/t\}$ denotes the unknown boundary values; either being a displacements or tractions. For example, for free edge plate, this vector contains unknown values of boundary displacements. The vectors $\{P\}$ and $\{u_c\}$ contain unknown values of interaction forces between the plate domain and the underneath elastic half space and the unknown displacements at the centers of internal soil cells respectively. The [0] and the $[I]$ are the zero and the identity matrices respectively. It has to be noted that if the plate is loaded by domain loading or series of patch or concentrated loadings, the effect of such loadings will be included in the vectors $\{RHS_b\}$ and $\{RHS_c\}$.

Recall the previous Section (2.3), the unknown values of interaction forces between the plate domain and the underneath elastic half space could be expressed in terms of the previously derived stiffness matrix for the elastic half space, i.e.

$$\{P\}_{3N_c\times 1} = [K]_{3N_c\times 3N_c}\{u_c\}_{3N_c\times 1} \tag{15}$$

Substituting Eq. (15) into Eq. (14) gives

$$\begin{bmatrix} [A]_{3N\times 3N} & [[A_2][K]]_{3N\times 3N_c} \\ [A_1]_{3N_c\times 3N} & [[I]+[A_3][K]]_{3N_c\times 3N_c} \end{bmatrix} \begin{Bmatrix} \{u/t\}_{3N\times 1} \\ \{u_c\}_{3N_c\times 1} \end{Bmatrix} = \begin{Bmatrix} \{RHS_b\}_{3N\times 1} \\ \{RHS_c\}_{3N_c\times 1} \end{Bmatrix} \tag{16}$$

Eq. (16) could be solved to obtain the unknown boundary values and internal displacement of the plate or the elastic half space.

Elastic half space forces could be computed easily using Eq. (15). Generalized displacements at any arbitrary internal point ξ could be obtained using Eq. (13) by replacing Y by ξ. Stress resultants (bending moments $M_{\alpha\beta}$ and shear forces $Q_{3\beta}$) could be also computed at any internal field point ξ by modifying the integral equations in Ref. [17] to include the effect of the elastic half space forces, to give

$$M_{\alpha\beta}(\xi) = \int_{\Gamma(x)} U_{\alpha\beta k}(\xi,x)t_k(x)d\Gamma(x) - \int_{\Gamma(x)} T_{\alpha\beta k}(\xi,x)u_k(x)d\Gamma(x) + \sum_c \left\{ P_3(y)\int_{\Omega_c(y)} \left[U_{\alpha\beta 3}(\xi,y) - \frac{v}{(1-v)\lambda^2} U_{\alpha\beta\theta,\theta}(\xi,y) \right] d\Omega_c(y) \right\} \tag{17}$$

and

$$Q_{3\beta}(\xi) = \int_{\Gamma(x)} U_{3\beta k}(\xi,x)t_k(x)d\Gamma(x) - \int_{\Gamma(x)} T_{3\beta k}(\xi,x)u_k(x)d\Gamma(x) + \sum_c \left\{ P_3(y)\int_{\Omega_c(y)} \left[U_{3\beta 3}(\xi,y) - \frac{v}{(1-v)\lambda^2} U_{3\beta\theta,\theta}(\xi,y) \right] d\Omega_c(y) \right\} \tag{18}$$

Eq. (17) and (18) were presented according to the formulation discussed in Ref. [20].

4. Numerical examples

In order to verify the present BEM elastic half space formulation, several examples including square, rectangular and circular plates under concentrated or distributed loads are considered. The displacement results obtained from the presented technique are compared to similar results obtained from previously published results based on different analytical and numerical approaches. Only Mindlin and Steinbrenner results are presented, as Mindlin and Boussinesq solutions give very similar results. In the present models, the plate is modeled using 16 quadratic boundary elements and the number of used Gauss points is 10 for numerical integration purposes along the boundary and 10×10 points for integration over domain cells.

4.1. Comparison to the Ritz method (Wang et al. [12])

The displacement results obtained from the present models are compared to those obtained from Ritz method presented in Ref. [12], which considers results based on both the Mindlin plate theory (MPT) and the classical thin plate theory (CPT).

Only square plates are demonstrated in the examples in this section. The considered plates are of uniform thickness h, width B, modulus of elasticity E_r and Poisson's ratio v_r, and resting on an elastic half space of modulus of elasticity E_s and Poisson's ratio v_s with infinite depth. The plate-soil stiffness ratio K_{rs} used by Fraser and Wardle [27] is re-used in the comparison herein where $K_{rs} = 4E_r(1-v_s^2)h^3/3E_s(1-v_r^2)B^3$. In the present models, 91 internal points are used to calculate results along the plate centerline.

4.1.1. Plate under central concentrated load

A square plate subjected to a central concentrated load P is considered. Fig. 2 demonstrates the displacement parameters, $I_w = E_s wB/[P(1-v_s^2)]$, along the centerline of the plate with the following parameters: $h/B=0.133$, $v_r=0.15$, $K_{rs}=0.126$ and $v_s=0.15$. It has to be noted that, in the present models, the soil is divided into 81 stiffness cells.

It can be seen that all results are in excellent agreements. The difference between the present models and the Ritz-MPT model compared to the Ritz-CPT model demonstrates the effect of the plate shear deformation.

4.1.2. Plate under uniformly distributed load

A square plate subjected to a uniformly distributed load p_r is considered. Fig. 3 demonstrates the variations of the displacement parameter, $I_w = E_s w/[p_r B(1-v_s^2)]$, along the centerline of the plate for various K_{rs} values and $h/B=0.15$. In the present models, the soil is divided into 961 stiffness cells. It can be seen that all results are in good agreement.

4.1.3. Plate under central square patch load

A square plate subjected to a central square patch load is considered. The size of the central patch load is defined by the parameter c/B. Figs. 4–6 demonstrate the variations of the displacement parameter, $I_w = E_s w/[p_r B(1-v_s^2)]$, along the plate centerline for various K_{rs} values and for $c/B=0.25$, 0.50 and 0.75,

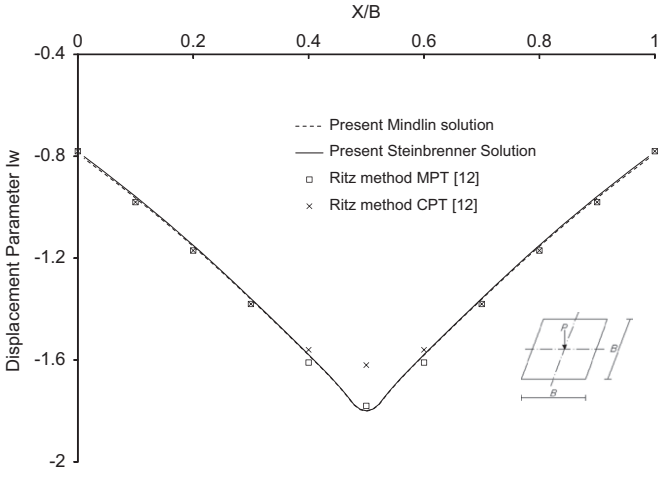

Fig. 2. Displacement distribution for a centrally concentrated loaded square plate.

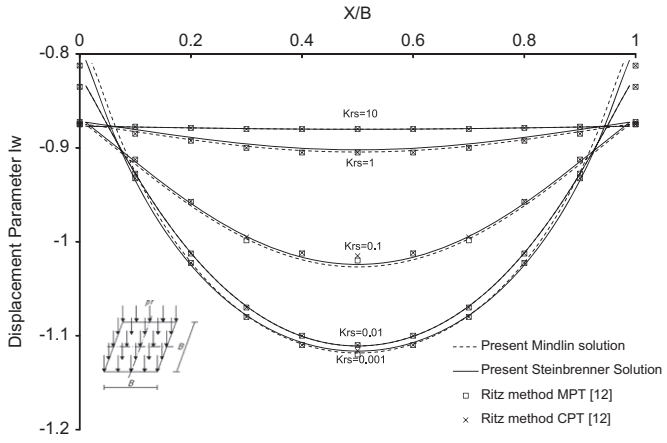

Fig. 3. Displacement distribution for a uniformly distributed loaded square plate.

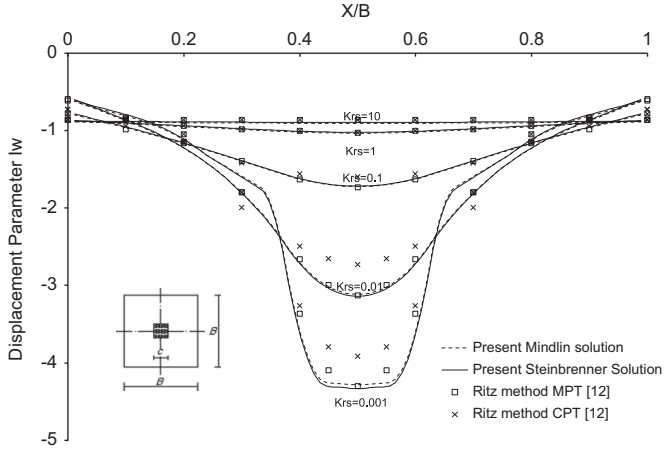

Fig. 4. Displacement distribution for a centrally patch loaded square plate with $c/B=0.25$.

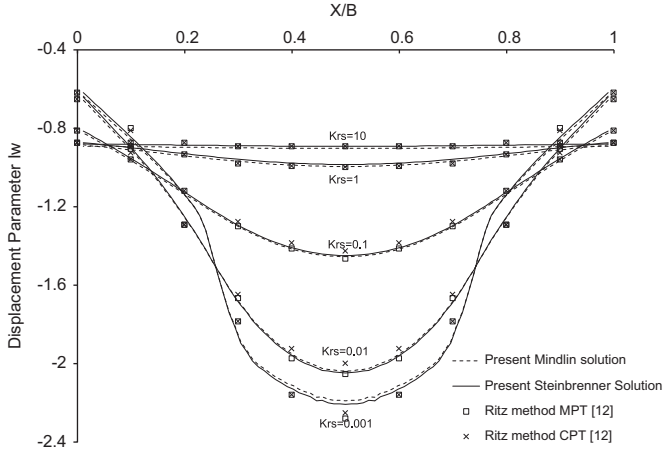

Fig. 5. Displacement distribution for a centrally patch loaded square plate with $c/B=0.50$.

respectively where the value of the plate constant h/B is 0.15. In the present models, the soil is divided into 81 stiffness cells.

It can be seen that all results are in good agreement. A very small value of c/B is equivalent to concentrated load, whereas, a large value of c/B can be regarded as a uniformly distributed load. The effect of the plate shear deformation is obvious in the Ritz-MPT model and in the present models rather than the Ritz-CPT model for low values of K_{rs}.

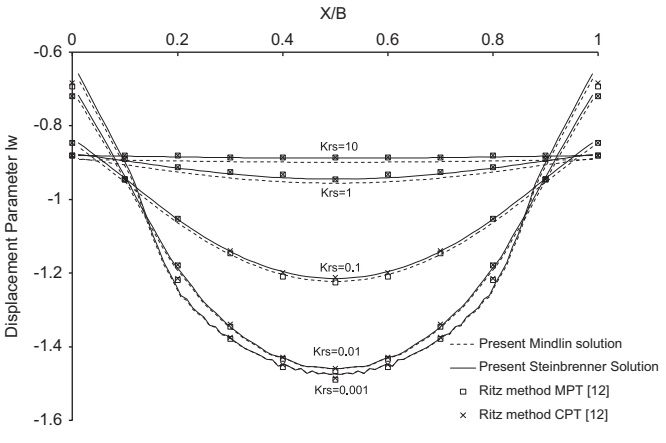

Fig. 6. Displacement distribution for a centrally patch loaded square plate with $c/B=0.75$.

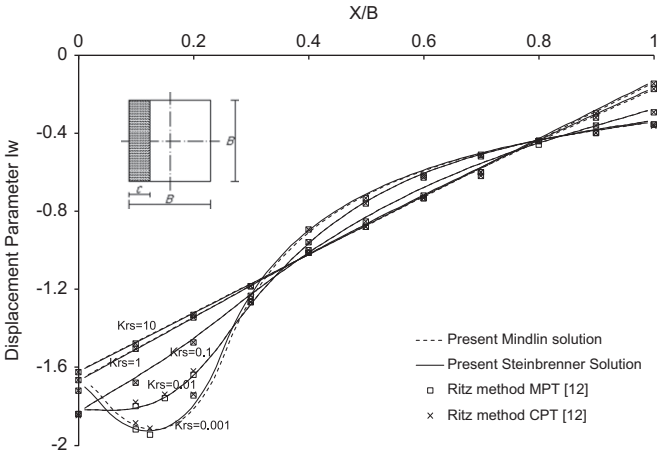

Fig. 7. Displacement distribution for a side-long patch loaded square plate with $c/B=0.25$.

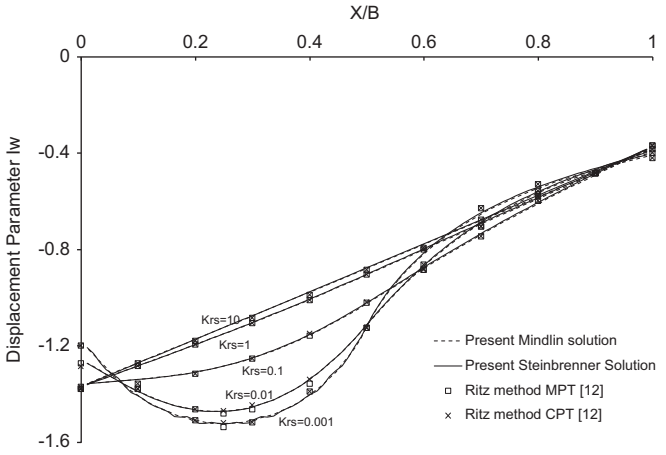

Fig. 8. Displacement distribution for a side-long patch loaded square plate with $c/B=0.50$.

4.1.4. Plate under side-long rectangular patch load

A square plate subjected to a side-long rectangular patch load is considered. The size of the side-long patch load is defined by the parameter c/B. Figs. 7–9 demonstrate the variations of the displacement parameter, $I_w = E_s w/[p_r B(1-\nu_s^2)]$, along the plate centerline for various values K_{rs} and for $c/B=0.25$, 0.50 and 0.75, respectively where the value of the plate constant h/B is 0.15.

It has to be noted that, in the present models, the soil is divided into 961 stiffness cells.

It can be seen that, all results are in good agreement. Similar conclusions could be drawn a those in Section (4.1.3).

4.2. Comparison to the formulation of Syngellakis and Bai [30]

In this example, the displacement results obtained from the present models are compared to those obtained from the BEM analysis of thin plate on Boussinesq half space reported by Syngellakis and Bai [30].

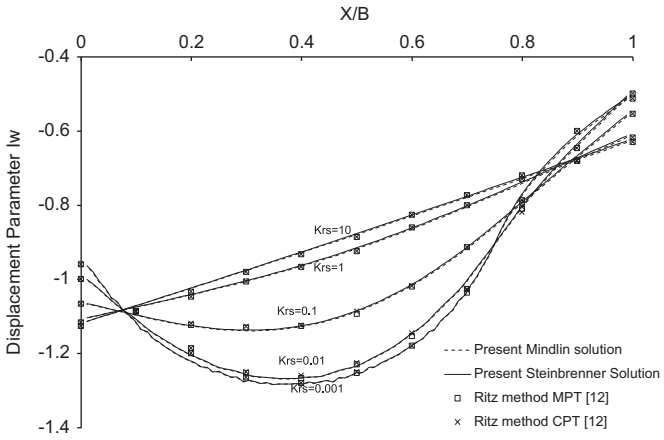

Fig. 9. Displacement distribution for a side-long patch loaded square plate with $c/B=0.75$.

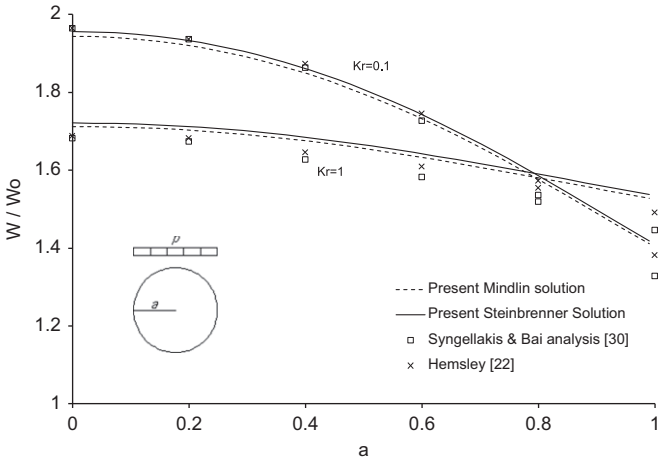

Fig. 10. Displacement distribution for a circular plate under uniform load.

A circular plate with free edge boundary condition and subjected to a uniform load p is considered. The plate has a uniform thickness h, radius a, modulus of elasticity E_r, Poisson's ratio ν_r, and resting on an infinite elastic half space of modulus of elasticity E_s and Poisson's ratio ν_s.

The plate-soil stiffness ratio used in this comparison is $K_r = E_r(1-\nu_s^2)h^3/E_s(1-\nu_r^2)a^3$.

The values: $h=0.1$ m, $a=1$ m, $E_s=21$ MPa, $\nu_r \times \nu_s = 0.2$ are used in the comparison.

In the present models, the soil is modeled using three meshes. The numbers of stiffness cells used are 97, 177, and 277 for meshes 1, 2 and 3 respectively. Twenty-eight internal points are used to calculate results along the plate centerline.

Fig. 10 demonstrates the displacement results of the present models using both of Mindlin and Steinbrenner solutions based on mesh 2. These results are compared to those of Syngellakis and Bai [30] together with previous predictions of hybrid finite-surface element scheme by Hemsley [22]. Table 1 demonstrates the displacement results for the above-mentioned numerical models and the analytical theoretical predictions for plates with negligible rigidity ($K_r=0$) and another time with infinite rigidity ($K_r=\infty$) analyzed by Timoshenko and Goodier [24]. It has to be noted that, the computed displacement is divided by the quantity $W_o = pa(1-\nu_s^2)/E_s$ to allow dimensionless comparisons.

It can be seen that all results are in good agreement. The present models are a bit closer to results given by Hemsley [22], which confirms the accuracy and the validity of the present formulation.

4.3. Comparison to the finite layer formulation of Ta and Small [14]

A uniformly loaded rectangular plate and a square plate under four concentrated loads are presented in this example. The present Mindlin and Steinbrenner solutions are considered and their results are compared to published results of Ta and Small [14], which considers FEM for plates on elastic half space solved by the finite layer method using two analyses: a full and an approximate analysis.

4.3.1. Rectangular plate under uniform load on infinite single-layered elastic half space

The plate demonstrated in this example is subjected to a uniform load of intensity p_r and has thickness h, length L and width B, where $L/B=2$. Modulus of elasticity is E_r and Poisson's ratio is ν_r. The plate is resting on an elastic half space of modulus of elasticity $E_s$and Poisson's ratio ν_s with infinite depth. The plate-soil stiffness ratio

Table 1
Displacement of a circular plate under uniform load.

Solution	$W(0)/Wo$				$W(a)/Wo$			
	$K_r=0$	$K_r=0.1$	$K_r=1$	$Kr=\infty$	$K_r=0$	$K_r=0.1$	$K_r=1$	$K_r=\infty$
Syngellakis and Bai [30] BEM mesh 1		1.972	1.663			1.309	1.408	
Syngellakis and Bai [30] BEM mesh 2		1.969	1.677			1.331	1.432	
Syngellakis and Bai [30] BEM mesh 3		1.964	1.68			1.329	1.439	
Hemsley [22]		1.96	1.685			1.363	1.465	
Timoshenko and Goddier [24]	2			1.57	1.273			1.57
Present Mindlin solution mesh 1	1.967	1.942	1.708	1.577	0.783	1.4	1.519	1.578
Present Mindlin solution mesh 2	1.977	1.944	1.712	1.583	1.228	1.411	1.528	1.585
Present Mindlin solution mesh 3	1.983	1.943	1.719	1.597	1.338	1.425	1.543	1.6
Present Steinbrenner solution mesh 1	1.984	1.959	1.72	1.588	0.79	1.409	1.531	1.59
Present Steinbrenner solution mesh 2	1.99	1.956	1.721	1.593	1.233	1.419	1.537	1.595
Present Steinbrenner solution mesh 3	1.994	1.953	1.726	1.605	1.343	1.431	1.551	1.607

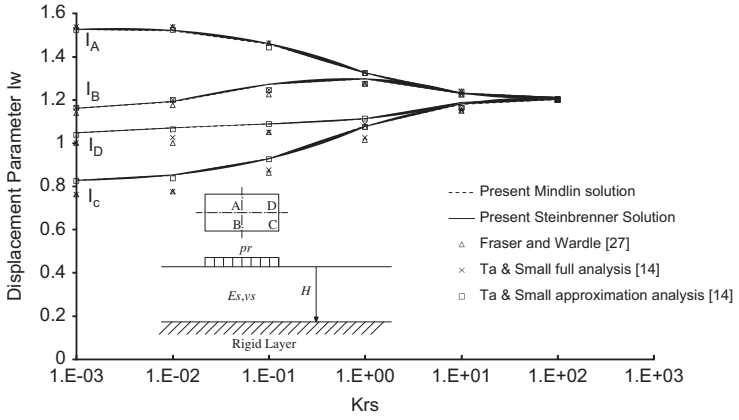

Fig. 11. Displacement distribution for a rectangular plate under uniform load at A, B, C and D.

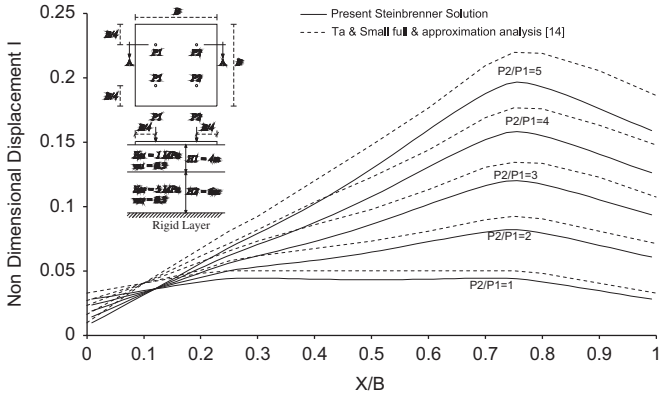

Fig. 12. Displacement distribution for a square plate under four concentrated loads along the strip A–A.

used in the comparison is $K_{rs}=4E_r(1-\nu_s^2)h^3/3E_s(1-\nu_r^2)B^3$. In the present models, the soil is divided into 496 stiffness cells.

Fig. 11 demonstrates the variations of the displacement parameter, $I_w=E_s w/[\,p_r B(1-\nu_s^2)]$ at points A, B, C and D (See Fig. 11) in the plate for various K_{rs} values. The displacement results obtained from the present models using both Mindlin and Steinbrenner solutions are compared to those results obtained from Ta and Small [14] as well as results analysis of Fraser and Wardle [27]. It can be seen that all results are in good agreement.

4.3.2. Square plate under four concentrated loads on two-layered elastic half space

The displacement results obtained from the present models using Steinbrenner solution are compared to those obtained from Ta and Small [14].

The plate demonstrated in this example is a square plate of uniform thickness $h=0.4$, length $B=12$ m, modulus of elasticity $E_r=3000$ and Poisson's ratio $\nu_r=0.2$. The plate is resting on a two-layered elastic half space and has a rigid end layer. The elastic parameters of each layer from the upper layer down to the lower one above the rigid layer are as follow:

Modulus of elasticity $E_{s1}=1$ MPa, Poisson's ratio $\nu_{s1}=0.3$ and thickness $H_1=4$ m.

Modulus of elasticity $E_{s2}=5$ MPa, Poisson's ratio $\nu_{s2}=0.3$ and thickness $H_2=6$ m.

The plate is loaded by four concentrated loads (two P_1 loads at the right and two P_2 loads at the left). Each load is located at a distance $B/4$ in both direction of X and Y from the nearest corner as demonstrated in Fig. 12.

In the present model, the soil is divided into 441 stiffness cells. Fifty-five internal points are used to calculate results along the column strip which includes both loads P_1 and P_2.

Fig. 12 demonstrates the effect of the load ratio P_2/P_1 on the non-dimensional displacement parameter $I=4wD_r/P_1B^2$ along the strip A–A (see Fig. 12), where w is the vertical displacement of the plate and, $D_r=\mathrm{E}_r h^3/[12(1-\nu_r^2)]$, is the flexure rigidity of the plate.

It can be seen from Fig. 12 that, the results of Steinbrenner solution in the present model are in a good agreement with those of Ta and Small [14].

4.4. Comparison to the work of Wang et al. [29]

Uniformly loaded square and trapezoidal plates resting on an elastic half space are considered herein. The present results are compared to those of Wang et al. [29].

4.4.1. Square plate under a uniform load and resting on infinite single-layered elastic half space

The displacement results obtained from the present models using both Mindlin and Steinbrenner solutions are compared to several referenced work including Wang et al. [29], the spline method [23], the displacement method [23] and the FEM for plate on half space [25].

The plate demonstrated in this example is subjected to a uniform load of intensity $p_r=0.98$ MPa and has thickness $h=0.2$ m and length $L=4$ m. Modulus of elasticity is $E_r=0.343\times10^5$ MPa and Poisson's ratio is $\nu_r=0.167$. The plate is resting on an elastic half space having modulus of elasticity $E_s=0.343\times10^3$ MPa and Poisson's ratio $\nu_s=0.4$ with infinite depth.

In the present models, the soil is presented with 3 meshes. In meshes 1, 2 and 3, the soil is divided into 4×4, 6×6 and 8×8 stiffness cells respectively. Table 2 demonstrates the computed displacements at the center point of the plate. It can be seen that all results are in good agreement.

4.4.2. Square plate under uniform load and resting on finite single-layered elastic half space

The displacement results obtained from the present models using both of Mindlin and Steinbrenner solutions are compared to those obtained from the analysis of Wang et al. [29] and the equivalent method presented in Ref. [27].

The plate demonstrated in this example is a square plate subjected to a uniform load of intensity $p_r=0.1$ MPa and has thickness $h=0.5$ m and length $L=10$ m. Modulus of elasticity is $E_r=0.15\times10^5$ MPa and Poisson's ratio is $\nu_r=0.2$. It is resting on

Table 2
Displacement at the center of a square plate under uniform load on an elastic half space.

	Spline method [23]	Displacement method [23]	FEM for plate on half space [25]	Wang et al. method [29]	Present Mindlin solution	Present Steinbrenner solution
Mesh (4 × 4)	0.01054	0.01054	0.01068	0.01045	0.01066	0.01085
Mesh (6 × 6)	0.01059	0.01059	0.01063	0.01052	0.01062	0.01074
Mesh (8 × 8)	0.01062	0.01062	0.01061	0.01060	0.01065	0.01075

Table 3
Displacement at the center, mid-edge and corner of a square plate on an elastic half space.

	Equivalent method [27]	Wang et al. method [29]	Present Mindlin solution	Present Steinbrenner solution
Center point	0.0107	0.0129	0.0103	0.0104
Mid-edge point	0.0078	0.0950	0.0083	0.0082
Corner point	–	0.0663	0.0066	0.0062

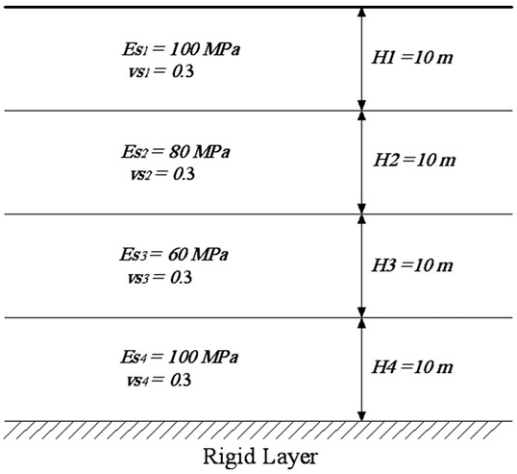

Fig. 13. Four-layered elastic half space.

a one-layered elastic half space of modulus of elasticity $E_s = 0.832 \times 10^2$ MPa, Poisson's ratio $\nu_s = 0.3$ and it has a rigid end layer at depth $H = 40$ m.

In the present models, the soil is divided into 64 stiffness cells. Table 3 demonstrates the computed displacements at the center, mid-edge and corner points of the plate. It can be seen from Table 3 that, the results of the present models are a bit closer to results given by the equivalent method [27], which confirms the accuracy and the validity of the present formulation.

4.4.3. Square plate under a uniform load and resting on multi-layered elastic half space

The displacement results obtained from the present models using both of Mindlin and Steinbrenner solutions are compared to those obtained from the analysis of Wang et al. [29] and both of the equivalent method in Ref. [27] and the numerical method in Ref. [26].

The plate demonstrated in this example is the same plate demonstrated in the previous Section (4.4.2). It is resting on four-layered elastic half space and it has a rigid end layer, (see Fig. 13). The elastic parameters for each layer starting from the upper layer down to the lower one above the rigid end layer are given as follow:

$E_{s1} = 100$ MPa, Poisson's ratio $\nu_{s1} = 0.3$ and thickness $H_1 = 10$ m.
$E_{s2} = 80$ MPa, Poisson's ratio $\nu_{s2} = 0.3$ and thickness $H_2 = 10$ m.

Table 4
Displacement at the center and mid-edge of a square plate on a multi-layered elastic half space.

	Equivalent method [27]	Numerical method [26]	Wang et al. method [29]	Present Mindlin solution	Present Steinbrenner solution
Center point	0.0107	0.0114	0.0120	0.0094	0.0097
Mid-edge point	0.0078	0.0870	0.0089	0.0076	0.0077

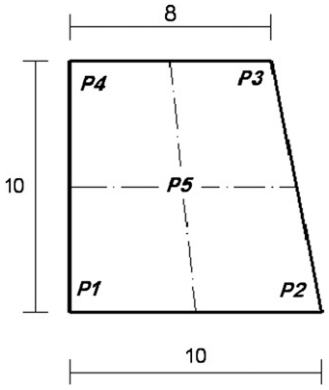

Fig. 14. Trapezoidal plate layout.

$E_{s3} = 60$ MPa, Poisson's ratio $\nu_{s3} = 0.3$ and thickness $H_3 = 10$ m.
$E_{s4} = 100$ MPa, Poisson's ratio $\nu_{s4} = 0.3$ and thickness $H_4 = 10$ m.

It has to be noted that, the equivalent layer (according to Bowels [13]) to these layers gives $E_s = 0.832 \times 10^2$ MPa and $\nu_s = 0.3$, which are similar values to those used in Section (4.4.2).

In the present models, the soil is divided into 64 stiffness cells. Table 4 demonstrates the computed displacements at the center and mid-edge points of the plate.

It can be seen that all results are in good agreement. The present results in the current example are a bit less than those obtained from the equivalent layer in the previous Section (4.4.2) because of the presence of a strong top soil layer. This could be overcome by considering more refined layering system, which is out of the scope of the present work.

4.4.4. Trapezoidal plate under uniform load and resting on finite single-layered elastic half space

The displacement results are compared to those obtained from the analysis of Wang et al. [29].

The trapezoidal plate demonstrated in Fig. 14 is considered in this example. The plate is subjected to a uniform load of intensity $p_r = 1$ MPa and has thickness $h = 2$ m, modulus of elasticity is $E_r = 0.26 \times 10^5$ MPa and Poisson's ratio is $\nu_r = 0.167$. The plate is resting on a single-layered elastic half space with modulus of elasticity $E_s = 0.26 \times 10^3$ MPa and Poisson's ratio $\nu_s = 0.25$ and with a rigid end layer at depth $H = 50$ m.

Table 5
Displacement at different points on a trapezoidal plate on an elastic half space.

	Wang et al. method [29]	Present Mindlin solution	Present Steinbrenner solution
Point P1	0.0244	0.0260	0.0256
Point P2	0.0254	0.0255	0.0250
Point P3	0.0220	0.0268	0.0263
Point P4	0.0226	0.0259	0.0255
Point, P5	0.0260	0.0280	0.0276

In the present models, the soil is divided into 811 stiffness cells. Table 5 demonstrates the computed displacements at the points P_1, P_2, P_3, P_4 and P_5 (shown in Fig. 14). It can be seen that all results are in good agreement.

5. Conclusions

In this paper, a new boundary element formulation for analysis plates resting on elastic half space was presented. In this formulation, the considered plate was modeled using the shear deformable plate bending theory. The soil flexibility matrix under arbitrary shaped plates was computed using elastic solutions of Boussinesq, Mindlin and Steinbrenner. Then, this flexibility matrix was inversed to get the soil stiffness matrix. This stiffness matrix was incorporated inside a developed BEM that accounts for the underneath elastic half space.

Several numerical examples were considered and the obtained results were compared against previously published analytical and numerical methods. It was demonstrated that, results of the present formulation are in good agreement with those obtained from other analytical and numerical methods.

The present formulation could be used in structural engineering practice. As an additional advantage of the present formulation is, it can be straightforward extended to analyze displacement of adjacent foundation plates due to adjacent newly constructions, which will be considered in a future research.

References

[1] Winkler E. Die lehr von elastizität und festigkeit. Dominicus: Prague 1867, pp. 182–4.
[2] Horvath JS. New subgrade model applied to mat foundations. ASCE. J Geotech Eng 1983;109(12):1567–87.
[3] Filonenko-Borodich MM. Some approximate theories of elastic foundation. Uch Zap Mosk Gos Uni Mekh 1940;46:3–18 [in Russia].
[4] Filonenko-Borodich MM. A very simple model of an elastic foundation capable of spreading the load. Sb Tr Mosk Elektro Inst Inzh Trans. Transzheldorizdat, vol. 53. Russia; 1945.
[5] Hetenyi M. Beams on elastic foundation. Ann Arbor, Michigan: University of Michigan Press; 1946.
[6] Pasternak PL. On a new method of analysis of an elastic foundation by means of two foundation constants. Gosudartvennoe Izdatelstro Liberaturi po Stroitelstvui Arkhitekture. Moscow, Russia; 1954.
[7] Kerr AD. Elastic and viscoelastic foundation models. J Appl Mech ASME 1964;31:491–8.
[8] Reissner E. Deflection of plates on viscoelastic foundation. J. Appl. Mech ASME 1958;80:144–5.
[9] Vlasov VZ, Leontiev UN. Beams, plates and shells on elastic foundations. Israel Program for Scientific Translation. Jerusalem [Translated from Russian]; 1966.
[10] ACI. Suggested analysis and design procedures for combined footings and mats. American Concrete Institute 336.2R-88; reapproved 2002.
[11] Selvadurai APS. Elastic analysis of soil foundation interaction. Amsterdam: Elsevier; 1979.
[12] Wang CM, Chow YK, How YC. Analysis of rectangular thick rafts on an elastic half space. Comput Geotech 2001;28:161–84.
[13] Bowels JE. Foundation analysis and design. 5th ed. New York: McGraw-Hill; 1996.
[14] Ta LD, Small JC. An approximation for analysis of raft and piled raft foundations. Comput Geotech 1997;20:105–23.
[15] Bézine G. Boundary integral formulation for plate flexure with arbitrary boundary conditions. Mech Res Commun 1978;5(4):197–206.
[16] Stern M. A general boundary integral formulation for the numerical solution of plate bending problems. Int J Solids Struct 1979;15:769–82.
[17] Vander Weeën F. Application of the boundary integral equation method to Reissner's plate model. Int J Numer Methods Eng 1982;18:1–10.
[18] Reissner E. On bending of elastic plates. Quart Appl Math 1947;5:55–68.
[19] Aliabadi MH, editor. Advanced in boundary element series, vol. 2. Southampton, UK: WIT press; 1998.
[20] Rashed YF. A boundary/domain element method for analysis of building raft foundations. Eng Anal Boundary Elem 2005;29:859–77.
[21] Das BM. Principles of geotechnical engineering. 5th ed. Canada: Thomson; 2002.
[22] Hemsley JA. Elastic solutions for axisymmetrically loaded circular raft with free or clamped edges founded on Winkler springs or a half-space. Proc Instit Civ Eng. 1987;83(part 2):61–90.
[23] Chen SJ, Peng YC. On spline finite element computation of plates on elastic foundations for various base-models. J Sun Yat-Sen Uni (Nat Sci Ed) 1980;2:15–23.
[24] Timoshenko SP, Goddier JN. Theory of elasticity. Singapore: McGraw-Hill; 1982.
[25] Wang YH, Qiu XM, Cheung YK. Bending plates on an elastic half-space analyzed by isoprametric elements. Chin J Geotech Eng 1998;20(4):7–11.
[26] Wardle LJ, Fraser RA. Finite element analysis of a plate on a layered cross-anisotropic foundation. In: Proceedings of the first international conference of finite element methods in engineering. Australia: University of New South Wales; 1974. p. 565–78.
[27] Fraser RA, Wardle LJ. Numerical analysis of rectangular rafts on layered foundations. Geotechnique 1976;26(4):613–30.
[28] Stavridis LT. Simplified analysis of layered soil-structure interaction. J Struct Eng 2002;128(2):225–6.
[29] Wang YH, Tham LG, Tsui Y, Yue ZQ. Plate on layered foundation analyzed by a semi-analytical and semi-numerical method. Comput Geotech 2003;30:409–18.
[30] Syngellakis S, Bai CX. On the application of the boundary element method to plate-half-space interaction. Eng Anal Boundary Elem 1993;12:119–25.
[31] Xiao JR. Boundary element analysis of unilateral supported Reissner plates on elastic foundations. Comput Mech 2001;27(1):1–10.
[32] Hu HC. Generalized variational principles in elasticity and its applications. Beijing, China: Science Press; 1982.